

Spectral CT with monochromatic imaging and metal artifacts reduction software for artifacts reduction of ^{125}I radioactive seeds in liver brachytherapy

Qiuxia Yang¹ · Sheng Peng¹ · Jing Wu¹ · Xiaohua Ban¹ · Mingyan He¹ ·
Chuanmiao Xie¹ · Rong Zhang¹

Received: 30 June 2015 / Accepted: 20 September 2015 / Published online: 11 October 2015
© Japan Radiological Society 2015

Abstract

Purpose To investigate the optimal monochromatic energy for artifacts reduction from ^{125}I seeds as well as image improvement in the vicinity of seeds on monochromatic images with and without metal artifacts reduction software (MARS) and to compare this with traditional 120-kVp images, so as to evaluate the application value of gemstone spectral imaging for reducing artifacts from ^{125}I seeds in liver brachytherapy.

Materials and methods A total of 45 tumors from 25 patients treated with ^{125}I seed brachytherapy in the liver were enrolled in this study. Multiphasic spectral computed tomography (CT) scanning was performed for each patient. After a delay time of 15 s of portal vein phase, a traditional 120-kVp scan was performed, focusing on several planes of ^{125}I seeds only. The artifact index (AI) in the vicinity of seeds and the standard deviation (SD) of the CT density of region of interest in the outside liver parenchyma were calculated. Artifact appearance was evaluated and classified on reconstructed monochromatic S and 120-kVp images. Image quality in the vicinity of seeds of three data sets were evaluated using a 1–5 scale scoring method. The Friedman rank-sum test was used to estimate the scoring results of image quality.

Results The greatest noise in monochromatic images was found at 40 keV (SD = 27.38, AI = 206.40). The optimal monochromatic energy was found at 75 keV, which

provided almost the least image noise (SD = 10.01) and good performance in artifact reduction (AI = 102.73). Image noise and AI reduction at 75 keV was decreased by 63.44 and 50.23 %, compared with at 40 keV. Near-field thick artifacts were obvious in all 45 lesions, in 120-kVp images, and 75-keV images, but basically reduced in 75 keV MARS images and artifacts completely invisible in 7 lesions. The number of diagnosable images (score ≥ 3) was significantly more in the 75-keV MARS group (28/45), and the 75-keV group (22/45) than in the 120-kVp group (11/45) ($p < 0.0167$ for both). Compared with 120-kVp images alone, 75-keV images plus 75-keV MARS images can increase tumor visibility around seeds and increase the proportion of diagnostic images to 84.4 % (38/45).

Conclusion Spectral CT producing 75-keV MARS images could substantially reduce near-field thick artifacts caused by ^{125}I seeds and improve image quality, even to a state of being completely free from artifacts. Spectral CT imaging (with and without MARS) can provide more accurate CT images for estimating efficacy after ^{125}I seed brachytherapy in the liver.

Keywords Artifacts reduction · Spectral computed tomography · Monochromatic imaging · Metal artifacts reduction software · ^{125}I seed brachytherapy

Introduction

Image-guided brachytherapy with ^{125}I radioactive seed implantation has been validated for promising efficacy and safety in previous studies and our own case records for malignant tumors in various locations of the body [1–8]. The American Brachytherapy Society (ABS) recommends that post-implant dosimetry should be performed on all

✉ Rong Zhang
yangqx@sysucc.org.cn

¹ State Key Laboratory of Oncology in South China, Department of Medical Imaging and Minimally Invasive Interventional Center, Sun Yat-sen University Cancer Center, 651 Dongfeng Road East, Guangzhou, Guangdong 510060, People's Republic of China

patients undergoing prostate brachytherapy. Computed tomography (CT)-based dosimetry is recommended, based on availability, cost, and the ability to visualize the prostate as well as the seeds [9]. In practice, CT-based dosimetry after ^{125}I seed brachytherapy is also widely used in many other locations of the body, including hepatic cancers. On the other hand, CT has also been one of the most important modalities for post-treatment efficacy assessment using the response evaluation criteria in solid tumors (RECIST, WHO) in many institutions. The ideal result of seed implantation is complete tumor dissipation, though we failed to accomplish such a good result in some cases. A decision to proceed with further intervention is most beneficial if residual or recurrent lesions are detected in time by radiology.

One of the few limiting factors are the prominent beam-hardening artifacts which result from ^{125}I seeds during CT scanning exactly in the vicinity of tumors. Artifacts not only blur the seeds but mask the tumor body, surrounding liver parenchyma, or even induce bright and dark streaks throughout the whole image in some cases. As a consequence, the diagnostic quality of the CT scan is compromised and the masked lesion might be missed. Reduction of these seed artifacts would improve tumor visualization and clear seed identification which is required for treatment evaluation and post-implant dosimetry.

The literature about artifact reduction for brachytherapy ^{125}I seeds is limited. Previous studies are mainly based on conventional CT imaging with various methods in both phantom and patient studies [10–15]. These described techniques vary in their ability to reduce seed artifacts while preserving tissue detail.

Recent advances in detector development have allowed spectral CT scanners to gain popular clinical use. One of the applications of spectral CT is reduction of beam-hardening artifacts, mainly by monochromatic imaging, and other metal-related artifacts by metal artifacts reduction software (S). In studies on several in vivo metal implants (e.g. prosthetic hip joint, artificial tooth, vascular clamp, and gold fiducial seeds), monochromatic images with and without MARS could obviously reduce the metal artifacts, and both the implants and surrounding structures were well displayed [16–21]. Based on previous observations, we speculated that spectral CT scanning could effectively remove brachytherapy seed artifacts as well. To our knowledge, data on artifact reduction for ^{125}I seeds in liver brachytherapy using spectral CT imaging is unavailable yet.

The purpose of this study was to investigate the optimal monochromatic energy for artifact reduction as well as image quality improvement in the vicinity of seeds on monochromatic images with and without MARS and to compare this with traditional 120-kVp images, so as to

evaluate the application value of gemstone spectral imaging (GSI) for reducing artifacts from ^{125}I seeds in the liver.

Materials and methods

Patient recruitment and CT imaging

A total of 25 patients who had received ^{125}I seed brachytherapy for 45 treated tumors in the liver were included in this study. Patient characteristics and treatment details are provided in Table 1. All post-implant follow-up CT images were acquired using a 64-detector CT scanner (GE Discovery CT750 HD, GE Medical Healthcare, Milwaukee, Wisconsin) at our institution during August 2012 to March 2013. All patients provided informed consent before inclusion in the study. Each patient underwent only one scheduled abdominal spectral CT exam after brachytherapy for this study. The median time interval between completion of seeds implantation and spectral CT scanning was 2 months (1–36.5).

Multiphase GSI scanning (i.e., nonenhanced, hepatic arterial, portal venous, and delayed phases) were performed for each patient. After a delay time of 15 s of portal vein phase, a traditional 120-kVp scan was performed, focusing on several planes of ^{125}I seeds only. The parameters of GSI were: tube voltage 140 and 80 kVp of 0.5 s instant switch, tube current 0–550 mA of automatic adjustment, collimation 0.625 mm, rotational speed 0.80 s, pitch 1.375, and volume-weighted CT dose index (CTDI_{vol}) 16.87 mGy. The parameters of traditional 120-kVp imaging were: tube current 300 mA, CTDI_{vol} 11.75–13.27 mGy (median 12.69 mGy), and the same other parameters as those of GSI. Contrast enhanced images were obtained after a bolus intravenous injection of 2.0 ml/kg of non-ionic contrast agent (Omnipaque 300, GE Healthcare, Shanghai, China) through a high-pressure syringe (Stellent dual-drum high-pressure syringe, Medrad Co., USA) at a rate of 3 ml/s.

Image reconstruction

The GSI data at portal vein phase was reconstructed with and without MARS, GE-specific software (Discovery CT750 HD, GE Medical Healthcare) on the scanner workstation. Then, all image data were imported into a post-processing workstation (GE Advantage workstation AW4.5; GE Medical Systems). The axial non-enhanced GSI images were reconstructed into 40- to 140-keV (kiloelectron-voltage) monochromatic images for 21 groups at an interval of 5 keV, at a slice thickness/interval of 2.5 mm. According to the preliminary results, the images at 75 keV provided less image noise and had good performance in

Table 1 Patient characteristics and treatment details

| | Total (<i>n</i> = 25 patients with 45 tumors) median (range) or number (%) |
|---|---|
| Age (<i>n</i> = 25) | 61 (29–77) |
| Gender (<i>n</i> = 25) | |
| Male | 18 (72 %) |
| Female | 7 (28 %) |
| Tumor histopathology (<i>n</i> = 25) | |
| Hepatocellular carcinoma | 10 (40 %) |
| Cholangiocellular carcinoma | 1 (4 %) |
| Metastasis | 14 (56 %) |
| 10 intestine cancer, 2 lung cancer, 1 melano carcinoma and 1 cervical carcinoma | |
| Tumor location (<i>n</i> = 45) | |
| S2 + 3 | 10 (22.2 %) |
| S4 | 6 (13.3 %) |
| S5 + 6 | 13 (28.9 %) |
| S7 + 8 | 16 (35.6 %) |
| Tumor size (mm) | 20 (15–36) |
| Tumors per patient | 1 (1–3) |
| Treatment (<i>n</i> = 45) | |
| ¹²⁵ I seed brachytherapy alone | 42 (93.3 %) |
| Previous TACE | 3 (6.7 %) |
| Seeds per tumor | 23 (9–42) |

S segment, TACE transcatheter arterial chemoembolization

artifact reduction. Consequently, the GSI data at portal vein phase was reconstructed into 75 keV monochromatic and 75 keV monochromatic + MARS images (75-keV MARS image). The monochromatic, MARS and 120-kVp images were reformed in axial, coronal and sagittal image planes, respectively with slice thickness/intervals of 2.5 mm. With experience, the image processing takes about 5 min and simplifies the previous workflow.

Artifact appearance measures

For GSI non-enhanced scan, the artifact index (AI) in the vicinity of seeds with 10 mm width and the standard deviation (SD) of the CT density of region of interest (ROI) in the outside liver parenchyma with no artifacts but closest to the seeds were used as metrics to select the optimal monochromatic energy providing better image quantification.

Images with single seeds, clusters of 2–3 seeds, or with ≥ 2 sites in the same plane without mutual interference of artifacts (a spacing distance of at least about 20 mm) were selected as measurable plane samples. Figure 1 illustrates manually setting ROIs around the seed and in the liver parenchyma free from artifacts: a doughnut-shaped ROI was obtained of 10-mm width. CT density of ROIs was automatically measured three times, then the pixel values of doughnut-shaped ROIs were separated out, the SDs calculated, and the mean

of three measurements recorded as the quantitative data for both ROIs, at all the 21 monochromatic energies (40–140 keV), in each measurement sample. The AI and its unit variation value (ΔAI), referring to the degree of artifact reduction, were calculated, $AI = (SD_1^2 - SD_2^2)^{1/2}$, $\Delta AI = (AI_1 - AI_2)/L$ (AI_1 : AI value at a low monochromatic energy; AI_2 : AI value at a high monochromatic energy; and L: interval value at the adjacent monochromatic energies, i.e. 5 keV).

Image quality analysis

The 75-keV monochromatic, 75-keV MARS and 120-kVp images were reviewed, observing the artifact's appearance and tumor visualization (tumor body, boundary or local liver parenchyma), slice by slice, in axial, coronal and sagittal planes, respectively. The seed artifacts were classified and image quality in the vicinity of seeds evaluated through the subjective scoring method.

Types of artifacts: A, near-field thick artifacts; B, near-field blurred artifacts + far-field stripy artifacts; C, far-field artifacts; and D, few or no artifacts. The visibility of the implanted tumor was graded according to a 1–5 scale as follows: 1, serious artifacts, and lesion completely or nearly completely invisible in all planes; 2, lesion invisible in axial plane, and partially visible (<50 %) in the coronal and sagittal planes; 3, lesion partially visible (<50 %) in axial plane, or mostly visible (>50 %)

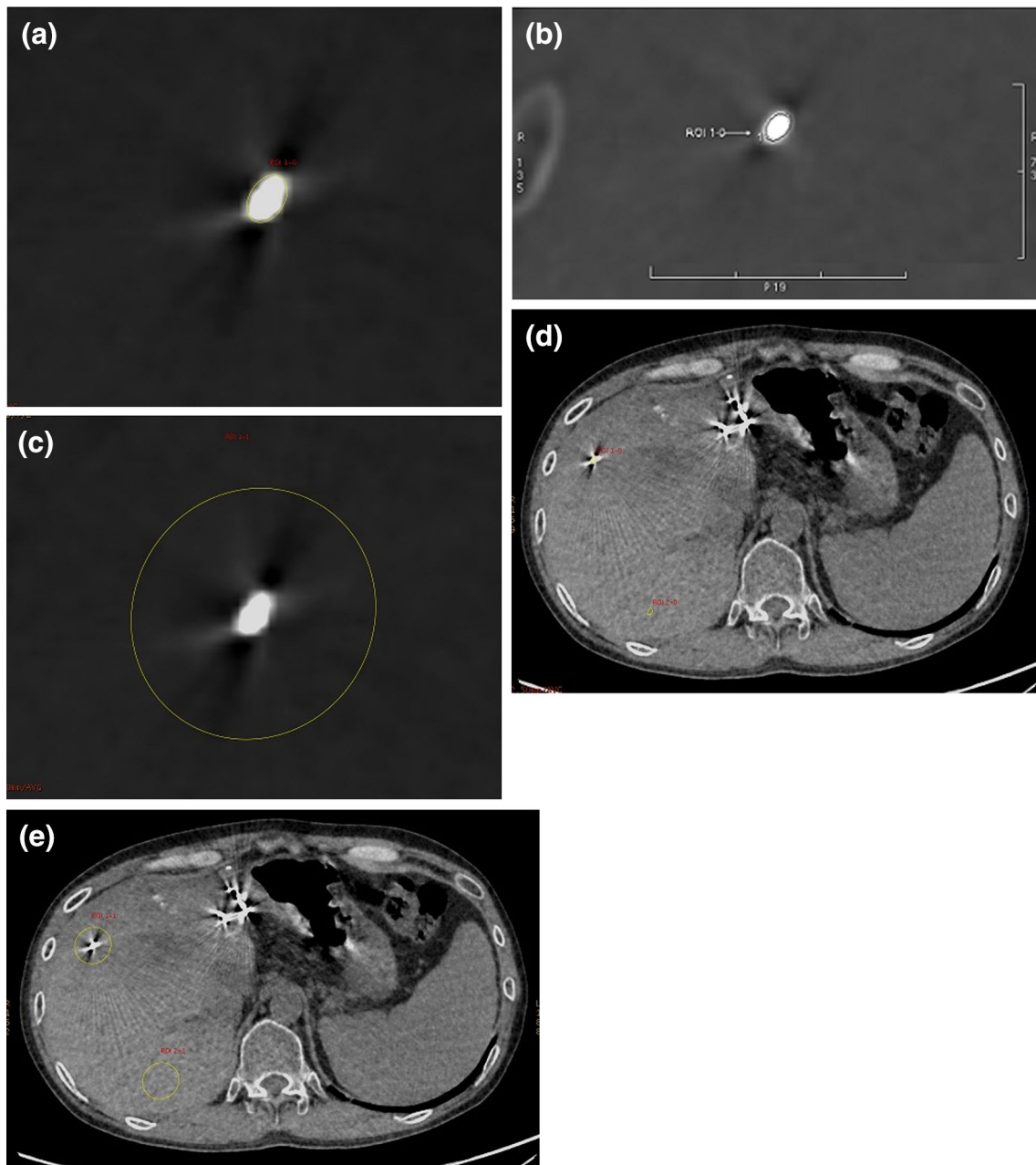


Fig. 1 Manual setting of ROIs around the seed and in the liver parenchyma. **a** At 140 keV, set the ROI in proper shape enclosing the seed, save as ROI₁₋₀. **b** Locally magnified, major diameter 4.5 mm and minor diameter 3.0 mm for ROI₁₋₀. **c** Increase the radius of ROI by

10 mm, save as ROI₁₋₁. **d, e** Adjust to 73 keV (default), duplicate the ROI₁₋₀ and ROI₁₋₁ to the outside liver parenchyma, save as ROI₂₋₀ and ROI₂₋₁. Then, pixel values of doughnut-shaped ROIs were got by removing those of the inner ROIs

in the sagittal and coronal planes; 4, few artifacts, and lesion visible (>50 %) in the axial images; and 5, no artifacts, and the whole lesion completely visible and well evaluated. With experience, the window width was set at 290 HU and window level at 50 HU for clearer identification of ¹²⁵I seeds and treated tumors. An image with a quality score ≥3 conformed to a diagnosable image or diagnosable lesion.

Statistical analysis

Results of continuous data were displayed as $\bar{x} \pm S$. The Friedman rank-sum test was used to estimate the scoring results of image quality and the Bonferroni method was used for the intra-group comparison. SPSS, version 17.0 (Chicago, IL) was used for statistical analysis. A $p < 0.05$ was considered to be statistically significant.

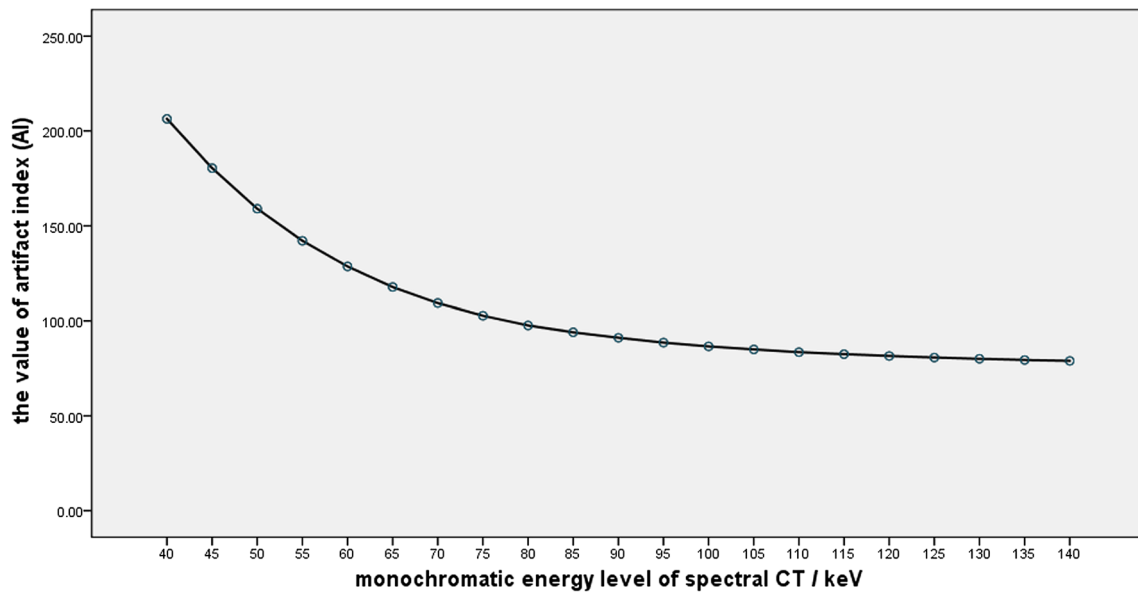


Fig. 2 Curve of mean AI value in the vicinity of seeds with 10-mm width

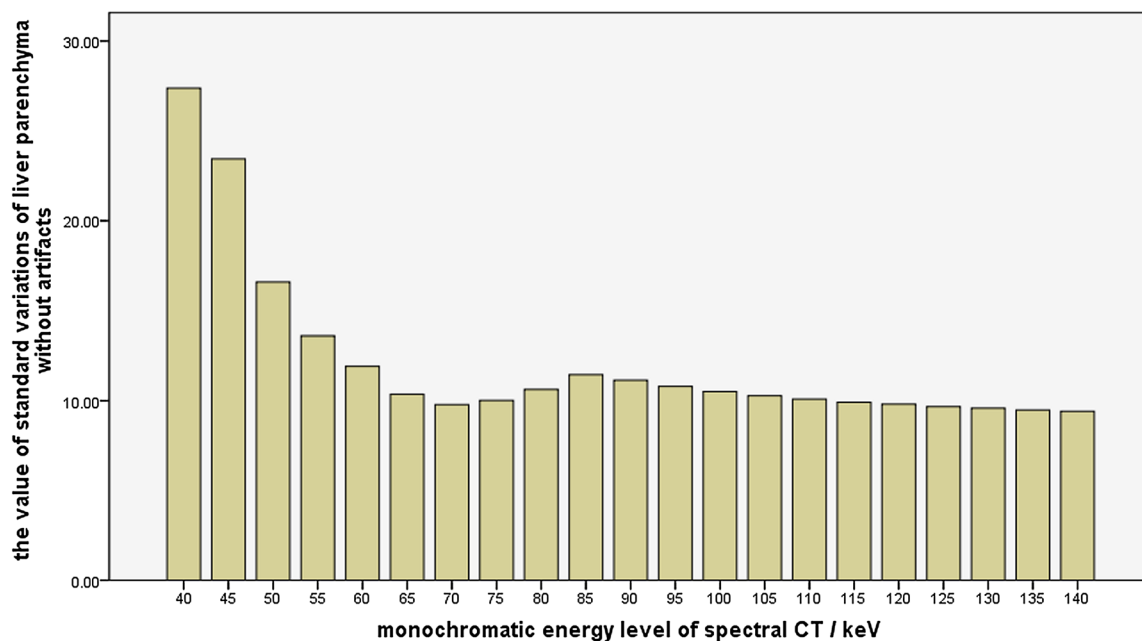


Fig. 3 Bar chart of noise (SD value) in the outside liver parenchyma with no artifacts

Results

Artifact appearance measures

A total of 48 plane samples were measured for CT density of ROIs. As displayed in Fig. 2, the AI value was maximal at 40 keV, and as the energy diverged from 40 keV, the AI

value gradually reduced from 206.40 ± 92.57 (AI_{40 keV}) to 78.96 ± 46.82 (AI_{140 keV}), indicative of more obvious artifact reduction with an increase in monochromatic energy. However, Δ AI decreased gradually from 5.20 to 1.02 (>1) at 40–75 keV and from 1.02 to 0.10 (<1) at 75–140 keV, indicative of a slighter magnitude of artifact reduction with an increase in monochromatic energy, and at 75 keV, Δ AI was 1.02.

Table 2 Measures of artifact appearance

| Mono energy | ROIs-1 ^a | | ROIs-2 ^b |
|-------------|---------------------|------------------|---------------------|
| | AI value | ΔAI ^c | SD value |
| 40 | 206.40 ± 92.57 | 5.20 | 27.38 ± 4.37 |
| 45 | 180.42 ± 82.43 | 4.28 | 23.44 ± 3.74 |
| 50 | 159.03 ± 73.60 | 3.38 | 16.59 ± 2.30 |
| 55 | 142.12 ± 66.68 | 2.70 | 13.60 ± 1.98 |
| 60 | 128.60 ± 61.64 | 2.17 | 11.91 ± 1.86 |
| 65 | 117.76 ± 57.84 | 1.69 | 10.35 ± 1.43 |
| 70 | 109.31 ± 55.04 | 1.32 | 9.78 ± 1.24 |
| 75 | 102.73 ± 52.94 | 1.02 | 10.02 ± 1.40 |
| 80 | 97.63 ± 51.39 | 0.72 | 10.63 ± 1.68 |
| 85 | 94.02 ± 50.25 | 0.58 | 11.44 ± 1.92 |
| 90 | 91.14 ± 49.39 | 0.51 | 11.14 ± 1.82 |
| 95 | 88.59 ± 48.77 | 0.40 | 10.79 ± 1.74 |
| 100 | 86.60 ± 48.31 | 0.32 | 10.50 ± 1.72 |
| 105 | 85.00 ± 47.96 | 0.29 | 10.27 ± 1.67 |
| 110 | 83.57 ± 47.67 | 0.21 | 10.09 ± 1.63 |
| 115 | 82.52 ± 47.46 | 0.19 | 9.91 ± 1.63 |
| 120 | 81.56 ± 47.28 | 0.16 | 9.80 ± 1.61 |
| 125 | 80.74 ± 47.13 | 0.13 | 9.67 ± 1.60 |
| 130 | 80.08 ± 47.01 | 0.12 | 9.59 ± 1.58 |
| 135 | 79.45 ± 46.90 | 0.10 | 9.48 ± 1.56 |
| 140 | 78.96 ± 46.82 | – | 9.41 ± 1.55 |

^a ROIs-1, ROIs in the vicinity of the seeds with 10 mm width
^b ROIs-2, ROIs in the outside liver parenchyma with no artifacts but closest to the seeds
^c ΔAI, unit variation value of AI

The maximum image noise (SD value) in liver parenchyma was seen at 40 keV, i.e. $SD_{40\text{ keV}} = 27.38$. The SD values were much smaller at the separate monochromatic energies of 70 and 140 keV, i.e. $SD_{70\text{ keV}} = 9.78 \pm 1.24$ and $SD_{140\text{ keV}} = 9.41 \pm 1.55$, as shown in Fig. 3.

At 75 keV, both the AI value and SD value were small, i.e. $AI_{75\text{ keV}} = 102.73 \pm 52.94$, $SD_{75\text{ keV}} = 10.02 \pm 1.40$: 50.23 and 63.44 % less than those values at 40 keV, respectively. Consequently, images at 75 keV provided fewer seed artifacts and less image noise with GSI non-enhanced scanning for ¹²⁵I seeds.

Artifact classifications

The artifact types and CT appearance are illustrated in Table 2 and Fig. 4. On 120-kVp images and 75-keV images, there were near-field thick artifacts at all 45 lesions (type A). The artifacts’ magnitude on 75-keV images was lower than that on 120-kVp images. Lesions were obscured and the surrounding liver parenchyma partially visible. On 75-keV MARS images, the near-field thick artifacts were

basically reduced in 45 lesions. The image series showed hardly artifacts but clear tumor visualization and seed identification in 7 lesions, as type D. The other two types were 25 lesions as B and 13 lesions as C. Additionally, artifact reduction using the MARS technique for images with separate seeds or a small number of seeds in the same plane was much better, showing a dense dot that represented almost the real size of the seed.

Evaluation of image quality in the vicinity of seeds

In the 75-keV MARS image group, the score of image quality was significantly higher than that in the 75-keV monochromatic group and the 120-kVp group, i.e. 2.92 ± 1.38 , 2.12 ± 1.19 and 1.61 ± 0.90 , respectively ($p = 0.002$), as shown in Table 3. The number of diagnosable lesions was 11 (24.44 %), 22 (48.89 %), and 28 (62.22 %) in the 120-kVp, 75-keV monochromatic, and 75-keV MARS group, respectively. In the 75-keV MARS group, 7 lesions were evaluated as 5 scores with no artifacts.

Compared with that in the 120-kVp group, the proportion of diagnosable lesions increased significantly by 37.78 and 24.44 % in 75-keV MARS group and the 75-keV monochromatic group, respectively (17/45, $p < 0.0167$; 11/45, $p < 0.0167$). The number of diagnosable lesions changed the most between the 75-keV monochromatic and 75-keV MARS group as shown in Table 4 and Figs. 5 and 6, while the score of image quality was not significantly different between the two groups ($p > 0.0167$).

Tumor evaluation in the vicinity of seeds by using 75-keV monochromatic images plus 75-keV MARS images can increase the proportion of diagnosable lesions to 84.4 % (38/45), compared with that of 24.44 % (11/45) in the 120-kVp group alone, showing the greatest diagnostic ability (Table 5).

Discussion

Follow-up CT imaging is required for efficacy evaluation after ¹²⁵I seed brachytherapy in the liver tumors. Artifacts from ¹²⁵I seeds during CT scanning present exactly in the vicinity of seeds, resulting in insufficient seed identification and tumor visualization. Prominent star-burst artifacts can make tumor response evaluation using RECIST impossible in some cases. Hence, there is an important need for a method or modality that reduces the seed artifacts.

Monochromatic images obtained with spectral CT imaging can undergo monochromatic image extraction and MARS reconstruction [18, 22–24]. Monochromatic images with and without MARS reconstruction can reduce metal artifacts, which has been verified in several previous studies [19, 25, 26]. In this study, GSI was applied to reduce the

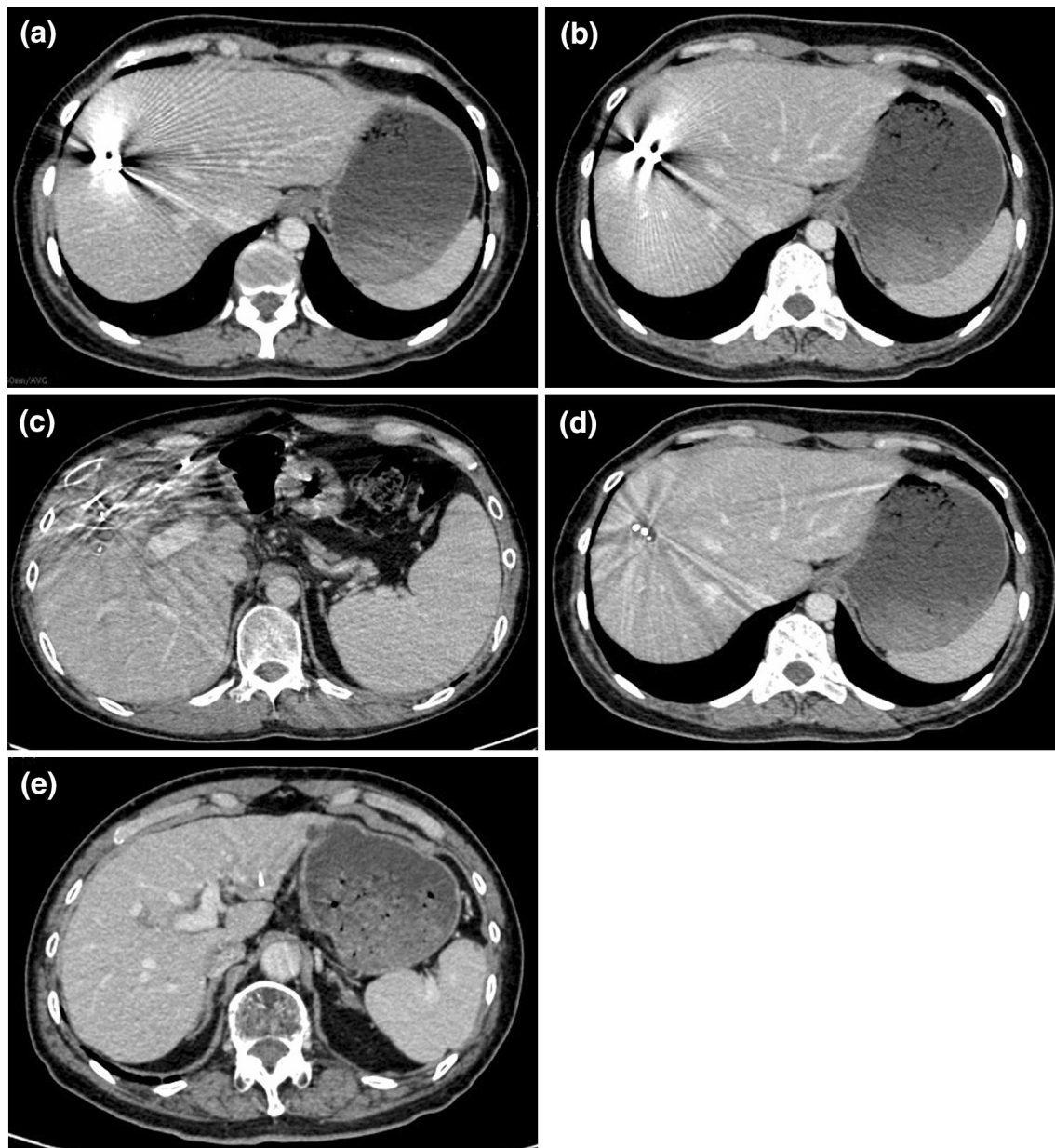


Fig. 4 Artifact types and CT appearance. Near-field thick artifacts on 120-kVp image (a) and 75-keV image (b), as type A; near-field blurred artifacts + far-field stripy artifacts on MARS image (c), as

type B; far-field artifacts on MARS image (d), as type C; no artifacts on MARS image (e), as type D

Table 3 Types of seed artifacts with GSI and 120-kVp imaging

| Type of image | Type of artifacts | | | |
|-------------------|-------------------|----|----|---|
| | A | B | C | D |
| 120-kVp image | 45 | 0 | 0 | 0 |
| 75-keV image | 45 | 0 | 0 | 0 |
| 75-keV MARS image | 0 | 25 | 13 | 7 |

Table 4 Image quality in the vicinity of seeds with GSI and 120-kVp imaging

| Type of image | Score of image quality | | | | | | Diagnostic images | |
|-------------------|------------------------|----|----|----|---|--------|-------------------|----------------|
| | 1 | 2 | 3 | 4 | 5 | Median | <i>n</i> | Proportion (%) |
| 120-kVp image | 17 | 17 | 9 | 2 | 0 | 2 | 11 | 24.44 |
| 75-keV image | 13 | 10 | 16 | 6 | 0 | 2 | 22 | 48.89 |
| 75-keV MARS image | 11 | 6 | 11 | 10 | 7 | 3 | 28 | 62.22 |

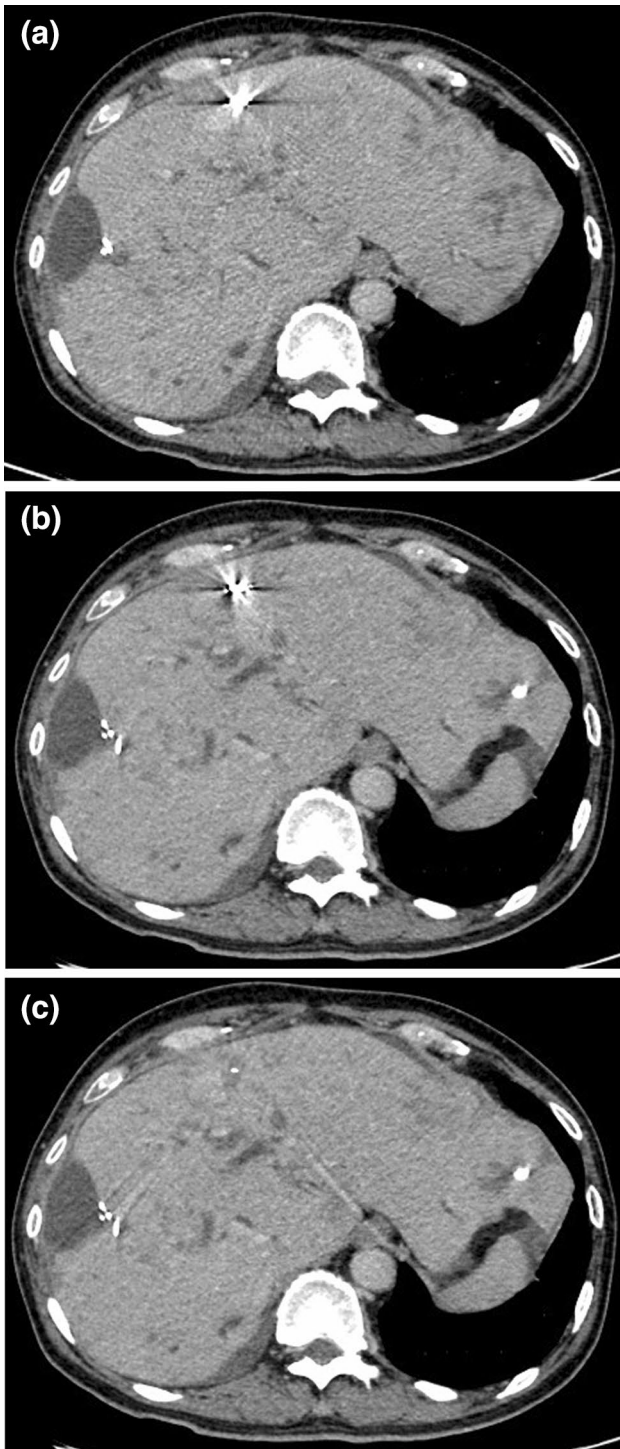


Fig. 5 Improved image quality on MARS image. **a** 120-kVp image and **b** 75-keV image: thick artifact in the vicinity of seeds. **c** MARS image: complete reduction of artifacts and score of 5

¹²⁵I seed artifacts in liver brachytherapy. We looked at the appearance and image quality of artifacts in 75-keV monochromatic images with and without MARS and compared

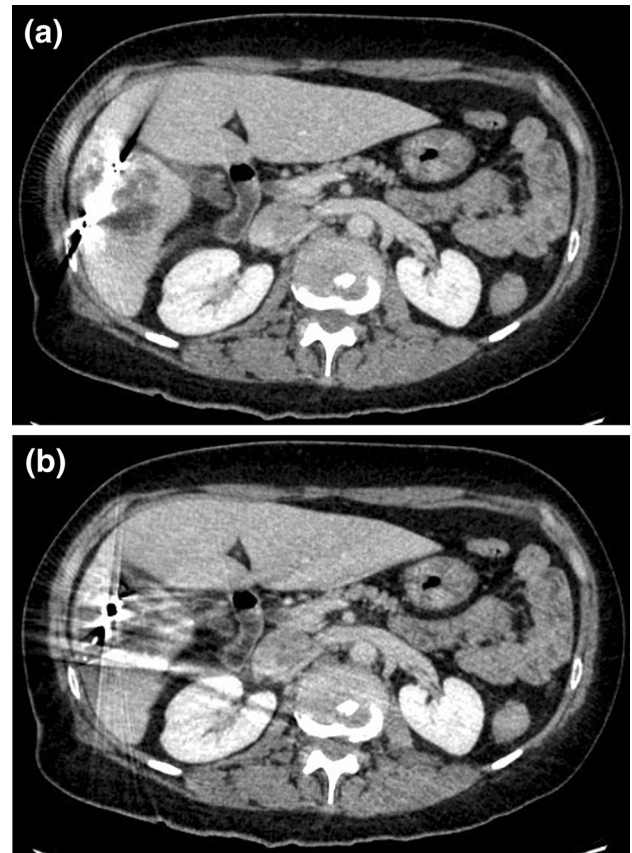


Fig. 6 Degraded image quality on MARS image. **a** 75-keV image: thick artifact in the vicinity of seeds, clear display of most tumor body and boundary (>50 %) in this plane. **b** MARS image: incomplete near-field artifacts reduction and many new stripy artifacts induced in far-field, unidentifiable tumor body and poorer image quality than before

that with 120-kVp images to assess whether monochromatic imaging reduced seed artifacts.

In monochromatic imaging by spectral CT with fast kilovoltage switching, i.e. at an instant 0.5 ms switch between 80 and 140 kVp, a projection-based beam-hardening correction can be performed because of the availability that two different kilovoltage peaks have for the same projection angle and the absorption of lower-energy X-rays can be changed that surpass the traditional polychromatic imaging [27]. So, the monochromatic imaging theoretically has no X-ray hardening effect [28], so as to overcome the hardening artifacts that exist at the traditional CT scanning.

In this study, the artifacts' magnitude was lower and the score of image quality was higher on 75-keV monochromatic images than that of 120-kVp images; monochromatic imaging demonstrated the ability to reduce seed artifacts caused by the ray absorptive hardening effect. In addition, the AI value was smaller as the values diverged from 40 keV, indicating that the higher the monochromatic energy, the more remarkable the artifact reduction, which is

Table 5 Number of diagnosable images with GSI and 120-kVp imaging

| Type of image | Number of diagnosable images | | |
|------------------------------------|------------------------------|----------|------------------|
| | Increase | Decrease | Total (increase) |
| 75-keV image vs 120-kVp image | 12 | 1 | 11 |
| 75-keV MARS image vs 120-kVp image | 21 | 4 | 17 |
| 75-keV MARS image vs 75-keV image | 16 | 10 | 6 |

in accordance with the previous practice of increasing the tube voltage in traditional CT scanning to mitigate metal artifacts and improve image quality [29–31]. This also agrees well with other research on monoenergetic imaging of dual-energy CT [18, 19, 26], although the degree of artifact reduction (ΔAI) gradually decreased with increase of monochromatic energy.

An optimal monochromatic energy exists that yields either the highest contrast-to-noise ratio (CNR) or lowest noise in the monochromatic image. As shown in studies by other groups [16, 24], the CNR was the largest at approximately 70 keV. As the X-ray energy values diverged from 70 keV, CNR decreased and the smallest was at 140 keV. Accordingly, images at 75 keV provide obvious seed artifact reduction, low noise and good performance of CNR while maintaining image integrity. Thus, 75 keV could be considered as the optimum monochromatic energy for post-process reconstruction for follow-up spectral CT imaging after ^{125}I seed brachytherapy. Published optimal monochromatic levels span a broad range depending on the type of metal implant (composition, size), CT protocol and imaging parameters, partitioning of the radiation dose between low- and high-energy scans, and the image quality metrics to be optimized [17, 24, 25], hence clinically applicable values should be determined locally.

MARS technology uses information from the spectral energy data set to segment regions of the detector that have photon starvation. It then determines the type of artifacts involved and corrects it by using an iterative reconstruction technique. Other researchers [19, 25] have said that evaluated image quality using GSI-MARS is subtly different, mainly being affected by implant composition and size, energy (in keV) as well as displayed fields-of-view (DFOV); our own observations agree with this view.

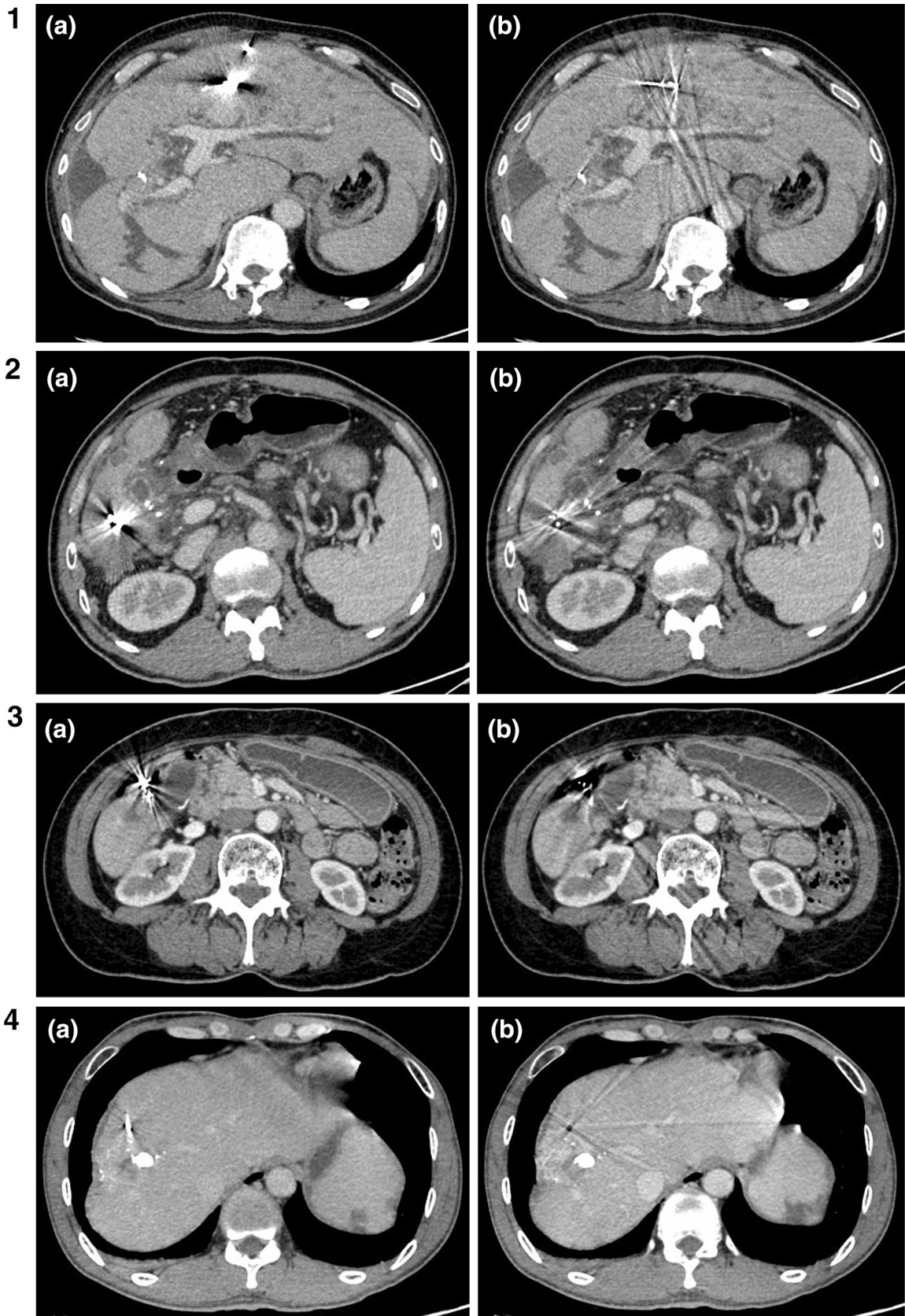
In this study, compared with the monochromatic image, the artifacts on the MARS images were more effectively reduced. The near-field thick seed artifacts of all 45 lesions were completely reduced, and the proportion of diagnosable lesions was obviously increased to 62.22 %; when combined with 75-keV monochromatic images, the proportion of diagnosable lesions was increased to 84.4 % (38/45). Consistent with our examined data of ^{125}I seeds, Brook et al. showed that MARS images provided better image quality than those with standard reconstruction in 60 % of patients (22/37) with gold fiducial seeds (5 mm in length),

which were placed in the vicinity of the tumor to aid the stereotactic radiation therapy [17]. MARS images obtained with spectral CT imaging demonstrate the same ability to reduce artifacts from small metal implants. Besides, seeds showed much more clearly with a demarcated contour, thereby facilitating the identification of seed number, and location. Accordingly, MARS images have potential for improving the accuracy of post-implant dosimetry.

Due to prominent near-field artifacts, there were a rather low proportion of diagnosable lesions, i.e. 11/45 in the 120-kVp image group in this study. In our clinical practice, the post-implant dosimetry might be inaccurately evaluated, but tumor response results should be reliable for the following reasons: firstly, the local recurrences were deemed based on sequential imaging findings, multidisciplinary group discussion, and eventual clinical outcome; and secondly and most importantly, the valid lethal distance of ^{125}I seed, i.e. 17 mm, was larger than the range of most artifacts, so the possible tumor lesions hidden behind artifacts could be deactivated with a sufficient radiation dose.

With monochromatic imaging and MARS reconstruction, the image quality was improved and worsened obviously alternately, and the number of diagnosable lesions was not significantly different between these two groups. Such conditions might be partially attributed to the following factors. Unlike the gold fiducial seeds used for stereotactic radiation therapy, there are one to three gold fiducial seeds in the vicinity of the treated tumors [17]. In principle, ^{125}I seeds are implanted into the liver at interval distance of 5–10 mm between individual seeds and 10–15 mm between brachytherapy catheters. The implanted seeds can amount to dozens in our maximum record. With the tumor dissolved, seeds become irregularly distributed or even clustered together so as to obviously restrict the effect of the MARS technique. The same feature was observed in another study, where artifacts caused by a small number of ^{125}I seeds were completely eliminated by a projection-interpolation method. Although artifacts from seeds in the same plane were mitigated, the contrast of images was degraded [10].

In our view, incomplete artifact reduction or new artifacts emerging with MARS reconstruction might also be related to the angle between the seed and the craniocaudal axis of the scanner, seed position and the high-density substances (deposited iodized oil) near seeds, as illustrated in Fig. 7.



◀ **Fig. 7** Incomplete artifacts reduction on MARS image and possible influencing factors. Some 75-keV images: near-field thick artifacts (**1a–4a**); MARS image: incomplete artifact reduction and induced new far-field stripy artifact or near-field extremely low-density gas-like shadow, possibly due to crossed orientation of seeds in the same plane and the angle between the seeds and the craniocaudal axis of the scanner (**1b**), the rib (**2b**), the colonic canal (**3b**) and overcorrection of seed artifacts (**4b**)

There was a trend toward more prominent artifacts with craniocaudal versus transverse orientation of the seed [17]. This may mean that more artifacts can be removed with the MARS algorithm when a larger volume of the seed is present in one section. This observation could be used for future seed placement so that seeds would be inserted preferentially in a transverse rather than a longitudinal orientation. Additionally, by regular seed placement with a precise interval as far as possible, there will be fewer artifacts in the MARS images with spectral CT imaging, although irregular seed clusters as a result of tumor diminishment after implantation is inevitable in reality. Artifact reduction through the MARS technique is also obviously influenced in such conditions, i.e. more far-field stripy artifacts would be induced for lesions adjacent to ribs and more near-field extremely low-density artifacts for lesions adjacent to intestines or liver top, in other words, close to tissue containing air. And MARS images showed poorly artifacts reduction for seeds inside of or near deposited iodized oil. Some seeds were hardly seen, or showed as a black spot, possibly due to the overcorrection of artifact reduction [17].

In this study, we have demonstrated the ability of monochromatic imaging with spectral CT with and without MARS to remove artifacts generated from ^{125}I seeds, and this has shown promising results. Besides improving image quality, monochromatic images have the potential for improving the accuracy of post-implant dosimetry. Thus, further validation of these results is needed with a following study on the dosimetry analysis using spectral CT imaging, and we have been doing the dosimetry evaluation using dose volume histograms after liver ^{125}I seeds brachytherapy.

Conclusion

In conclusion, monochromatic images at 75 keV demonstrate fewer seed artifacts and less image noise with GSI scanning for ^{125}I seeds. MARS images at 75 keV could substantially reduce near-field thick seed artifacts and improve image quality, even completely removing artifacts. Combining 75-keV images with 75-keV MARS images can provide the most diagnosable lesions. Spectral CT imaging can be considered for use at follow-up evaluation for patients with ^{125}I seed brachytherapy in the liver, and furthermore,

75-keV images with and without MARS post-process reconstruction would be a preferable recommendation.

Compliance with ethical standards

Conflict of interest The authors declare that they have no conflict of interest.

References

- Ricke J, Wust P. Computed tomography-guided brachytherapy for liver cancer. *Semin Radiat Oncol*. 2011;21:287–93.
- Wieners G, Pech M, Rudzinska M, et al. CT-guided interstitial brachytherapy in the local treatment of extrahepatic, extrapulmonary secondary malignancies. *Eur Radiol*. 2006;16:2586–93.
- Ricke J, Wust P, Stohlmann A, et al. CT-guided interstitial brachytherapy of liver malignancies alone or in combination with thermal ablation: phase I–II results of a novel technique. *Int J Radiat Oncol Biol Phys*. 2004;58:1496–505.
- Dickinson P, Malik J, Mandall P, et al. Five year outcomes following I-125 seed brachytherapy for low risk prostate cancer at three United Kingdom cancer centres. *BJU Int*. 2013;. doi:10.1111/bju.12358.
- Nag S, DeHaan M, Scruggs G, et al. Long-term follow-up of patients of intrahepatic malignancies treated with iodine-125 brachytherapy. *Int J Radiat Oncol Biol Phys*. 2006;64:736–44.
- Kimura T, Kido M, Miki K, et al. Mid-term outcome of permanent prostate iodine-125 brachytherapy in Japanese patients. *Int J Urol*. 2014;21:473–8.
- Zhang FJ, Li CX, Zhang L, et al. Short- to mid-term evaluation of CT-guided ^{125}I brachytherapy on intra-hepatic recurrent tumors and/or extra-hepatic metastases after liver transplantation for hepatocellular carcinoma. *Cancer Biol Ther*. 2009;8:585–90.
- Jiang Y, Huang ZL, Wu PH, et al. Short-term efficacy of CT-guided radioactive seed ^{125}I implantation on residual or relapsing metastatic lymph nodes in advanced tumor patients after multimodality treatment. *Ai Zheng*. 2008;27:1082–7.
- Nag S, Bice W, DeWyngaert K, et al. The American Brachytherapy Society recommendations for permanent prostate brachytherapy postimplant dosimetric analysis. *Int J Radiat Oncol Biol Phys*. 2000;46:221–30.
- Takahashi Y, Mori S, Kozuka T, et al. Reduction of computed tomography metal artifacts due to I-125 seeds for post implant analysis in prostate permanent brachytherapy. *Med Phys*. 2005;32:1960.
- Takahashi Y, Mori S, Kozuka T, et al. Preliminary study of correction of original metal artifacts due to I-125 seeds in postimplant dosimetry for prostate permanent implant brachytherapy. *Radiat Med*. 2006;24:133–8.
- Xu C, Verhaegen F, Laurendeau D, et al. An algorithm for efficient metal artifact reductions in permanent seed. *Med Phys*. 2011;38:47–56.
- Basran PS, Robertson A, Wells D. CT image artifacts from brachytherapy seed implants: a postprocessing 3D adaptive median filter. *Med Phys*. 2011;38:712–8.
- Sutherland J, Miksys N, Furutani KM, et al. Patient-specific Monte Carlo simulation of lung brachytherapy: metallic artifact reduction and organ-constrained tissue assignment. *Med Phys*. 2013;40:476.
- Sutherland JGH, Miksys N, Furutani KM, et al. Metallic artifact mitigation and organ-constrained tissue assignment for Monte

- Carlo calculations of permanent implant lung brachytherapy. *Med Phys*. 2014;41:011712.
16. Matsumoto K, Jinzaki M, Tanami Y, et al. Virtual monochromatic spectral imaging with fast kilovoltage switching: improved image quality as compared with that obtained with conventional 120-kVp CT. *Radiology*. 2011;259:257–62.
 17. Brook OR, Gourtsoyianni S, Brook A, et al. Spectral CT with metal artifacts reduction software for improvement of tumor visibility in the vicinity of gold fiducial markers. *Radiology*. 2012;263:696–705.
 18. Bamberg F, Dierks A, Nikolaou K, et al. Metal artifact reduction by dual energy computed tomography using monoenergetic extrapolation. *Eur Radiol*. 2011;21:1424–9.
 19. Lee YH, Park KK, Song HT, et al. Metal artefact reduction in gemstone spectral imaging dual-energy CT with and without metal artefact reduction software. *Eur Radiol*. 2012;22:1331–40.
 20. Xiao-li LI, Wei-hua F, Cheng D, et al. The experimental quantitative study of spectral CT imaging in reducing the metal artifacts. *Chin J Radiol*. 2011;45:736–9.
 21. Liang S, Mei-ai LI, Ji-hua L, et al. The best monochromatic imaging for reducing spinal metal artifacts with gemstone spectral imaging. *Chin J Med Imaging Technol*. 2011;27:1918–21.
 22. Yu L, Leng S, McCollough CH. Dual-energy CT-based monochromatic imaging. *AJR Am J Roentgenol*. 2012;199:S9–15.
 23. Cui Y, Gao SY, Wang ZL, et al. Which should be the routine cross-sectional reconstruction mode in spectral CT imaging: monochromatic or polychromatic? *Br J Radiol*. 2012;85:e887–90.
 24. Yu L, Christner JA, Leng S, et al. Virtual monochromatic imaging in dual-source dual-energy CT: radiation dose and image quality. *Med Phys*. 2011;38:6371–9.
 25. Zhou C, Zhao YE, Luo S, et al. Monoenergetic imaging of dual-energy CT reduces artifacts from implanted metal orthopedic devices in patients with fractures. *Acad Radiol*. 2011;18:1252–7.
 26. Meinel FG, Bischoff B, Zhang Q, et al. Metal artifact reduction by dual-energy computed tomography using energetic extrapolation: a systematically optimized protocol. *Invest Radiol*. 2012;47:406–14.
 27. Zhang D, Li X, Liu B. Objective characterization of GE discovery CT750 HD scanner: gemstone spectral imaging mode. *Med Phys*. 2011;38:1178–88.
 28. Silva AC, Morse BG, Hara AK, et al. Dual-energy (spectral) CT: applications in abdominal imaging. *Radiographics*. 2011;31(1031–1046):1047–50.
 29. Verburg JM, Seco J. CT metal artifact reduction method correcting for beam hardening and missing projections. *Phys Med Biol*. 2012;57:2803–18.
 30. Elstrom UV, Muren LP, Petersen JB, et al. Evaluation of image quality for different kV cone-beam CT acquisition and reconstruction methods in the head and neck region. *Acta Oncol*. 2011;50:908–17.
 31. Kovacs M, Fejerdy P, Dobo NC. Metal artefact on head and neck cone-beam CT images. *Fogorv Sz*. 2008;101:171–8.